Accepted final author manuscript. M. Hannula, J. A. K. Hyttinen, and J. M. A. Tanskanen, "Enhancing CT 3D images by independent component analysis of projection images," in J. Henriques, N. Neves., and P. de Carvalho (eds.) XV Mediterranean Conference on Medical and Biological Engineering and Computing – MEDICON 2019, Coimbra, Portugal, Sept. 2019. IFMBE Proceedings, vol 76. Springer, Cham, pp. 381–389. https://doi.org/10.1007/978-3-030-31635-8_46. © Springer Nature Switzerland AG 2020

Enhancing CT 3D Images by Independent Component Analysis of Projection Images

Markus Hannula[0000-0002-4485-8004], Jari A. K. Hyttinen[0000-0003-1850-3055], Jarno M. A. Tanskanen✉[0000-0001-7183-318X]

BioMediTech, Faculty of Medicine and Health Technology,
Tampere University, Arvo Ylpön katu 34, 33250 Tampere, Finland
markus.hannula@tut.fi, jari.hyttinen@tut.fi, tanskanen@ieee.org

Abstract. Computed tomography (CT) is an imaging modality producing 3D images from sets of 2D X-ray images taken around the object. The images are noisy by nature, and segmentation of the 3D images is tedious. Also, detection of low contrast objects may be difficult, if not impossible. Here, we propose an independent component analysis (ICA) based method to process sets of 2D projection images prior to 3D reconstruction to remove noise, and to enhance objects for detection and segmentation. In this paper, a proof-of-concept is provided: the proposed method was able to separate noise and image components, as well as to make visible objects that were not observable in 3D images without processing. We demonstrate our method in object separation with 2D slice image processing simulations, and by enhancing a 3D image of a polymer sample taken with Xradia MicroXCT-400. The method is applicable in any CT tomography for which a number of project image sets with different contrasts can be taken, e.g., in multispectral fashion.

Keywords: Computed Tomography, CT, μCT, Micro-CT, Independent Component Analysis, Image Processing, 3D Imaging.

1 Introduction

In this paper, we propose to enhance 3D computed tomography [1] (CT) images by independent component analysis (ICA) [2,3,4] based image processing. CT is an imaging modality in which 3D images are produced by a computational reconstruction algorithm from a set of normal 2D X-ray images taken at several angles around the object. Here, in the context of tomography, we call 2D X-ray images projection images. The number of projection images can vary from a few tens to thousands. In general, the more there are projection images, the better the resulting 3D image can be. Normal CT imaging considers usually objects of the size of the order of a human or organ, whereas μCT imaging considers imaging at resolutions of the order of micrometers. All common forms of CT are widely utilized in the image-based analysis of most any radiopaque objects, for example, bio- and industrial materials and their defects, biomaterial compositions, soils, ceramics, and biological tissues and cell constructs.

For CT 3D image reconstruction, good quality projection images are essential; they should be as noiseless and artefact free as possible. As a signal processing rule of thumb, noise and artefact reduction should be done as early as possible in the processing chain to provide the subsequent processing steps as good quality data as possible. Also, processing of 3D images would be computationally much more demanding than processing 2D images. Thus, we propose to enhance 3D μCT images by ICA-based preprocessing the projection images prior to 3D reconstruction.

In CT and X-ray contexts, ICA has previously been used, e.g., for X-ray coronary digital subtraction angiography [5] and removing X-ray scatter [6]. In this paper, we propose a general method to enhance any projection tomography images for which a number of projection image sets with different contrasts is available. We demonstrate the method by MATLAB (MathWorks, Natick, MA, USA) simulations, and by processing multispectral μCT images of polymer samples. This serves as a proof-of-concept of the proposed method.

2 Materials and Methods

2.1 Independent Component Analysis

The heart of ICA is to find independent source signals, i.e., the independent components (ICs) making up the measured signals or recordings. The ICA mixing model [2] is

$$\mathbf{Y}_i = \mathbf{A}_i\mathbf{X}_i \tag{1}$$

where the recordings in the rows of $\mathbf{Y}_i$ are linear combinations of the ICs in the rows of $\mathbf{X}_i$ with $\mathbf{A}_i$ being the mixing matrix and i (here, i = 1, …, 1600) is the index of the tomographic projection angle. Numerical iterative algorithms exist to find a separation matrix $\mathbf{B}_i = \mathbf{A}_i^{-1}$ so that the rows of $\mathbf{X}_i$ are mutually statistically independent (down to an error tolerance) based on $\mathbf{Y}_i$. The ICs are found by $\mathbf{X}_i = \mathbf{B}_i\mathbf{Y}_i$. In the sequel, we omit the index i when not referring to our particular application in which ICA is run a number of times.

For ICA, three assumptions must be satisfied [2]: 1) ICs exist, 2) measurements are linear combinations of the ICs (1), and 3) the ICs are non-Gaussian. Observing (1), three ambiguities concerning the ICs are evident: 1) the signs, 2) the energies, and 3) the order of appearance of the ICs in $\mathbf{X}$ are arbitrary. To see the ambiguities explicitly written out, and examples of time signal processing using ICA, see [10].

The intrinsic properties of ICA include that at most as many ICs can be found as there are measurements, and if there are more measurements than ICs, only at most the true number of ICs can be found. ICA can be powerful in recovering minor source signals and eliminating independent noise components. For full discussion, including the description of the ICA algorithm we use here, FastICA [7], see [2]. In this proof-of-concept paper, the choice of ICA algorithm is not important.

The main usages of ICA are 1) to find ICs carrying relevant source signals to utilize them directly, 2) to reconstruct the measurements using only the ICs carrying information of interest, or 3) to reconstruct the measurements omitting the ICs carrying noise

or other undesired signal components. Here, we are concerned with the cases 2 and 3. Zeroing the rows of **X** corresponding to the uninteresting or noise ICs to get **X'**, their contributions are eliminated when the measurements are reconstructed as

$$\mathbf{Y'} = \mathbf{AX'}. \tag{2}$$

The measurements and ICs can be any sets of values, such as time signals or images, satisfying the assumptions and (1). Relevant to this paper, note that (1) and nothing above is concerned with the order of samples in the measurements; the corresponding samples must only occur in the same locations in all the measurement vectors. I.e., image pixels can be arranged in the rows of **X** (1) in any order, as long as all the images are converted to vectors with the same pixel order.

Principal component analysis (PCA) [2,9] uses the same mixing model (1), but PCA has been devised from a different point of view: PCA finds uncorrelated components, which in general cannot be associated with source signals. PCA can be powerful, e.g., in noise and dimension reduction tasks [2,9].

2.2 ICA Usage

All the projection images taken at the same angle with the different CT parameters were collected in to one $\mathbf{Y}_i$ (1), one image per row, and FastICA was executed. This was done for each projection angle separately, i.e., FastICA was run 1600 times with different $\mathbf{Y}_i$s. Thereafter, the independent component images (ICIs) of interest were found in all $\mathbf{X}_i$, and the projection images were reconstructed using (2) with the unwanted ICIs zeroed in the $\mathbf{X}_i$'s. For noise removal, the unwanted ICIs are the ones consisting of (mostly) noise, and for image component separation, the unwanted ICIs can be all ICIs but the ones carrying information from the desired object. 3D reconstruction was then performed normally with the corresponding ICA-reconstructed and enhanced projection images $\mathbf{Y}_i$'. The entire process is illustrated in Fig. 1.

To comply with the ICA mixing model (1), the corresponding projection image pixels from the different imagings must carry X-ray attenuation due to the same material volume. Thus, the phantom remained fixed in the device between the imagings.

For ICA, there should be regions in the sample, whose image contributions change differently from those of the other regions with the changing imaging parameters. This could result from 1) absorption spectrum differences between the materials, 2) accumulation of contrast agent, 3) addition/removal of material, and/or 4) noise differences between the imagings.

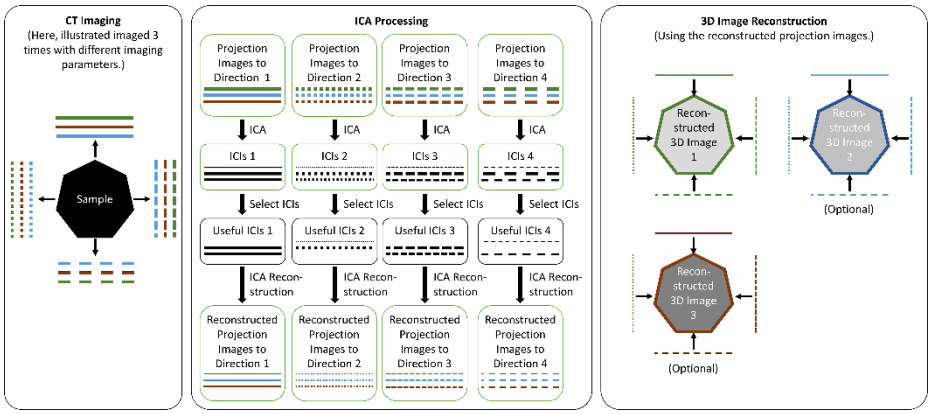

Fig. 1. The steps of the proposed method: CT imaging is performed a number of times with different imaging parameters. Next, ICA processing is applied to the projection images taken to any one direction. Then, ICIs carrying desired information are selected, or ICIs carrying undesirable components zeroed. In this step, it is necessary to identify the ICIs corresponding to each other between the different imaging directions, since the order of appearance of ICIs from ICA is arbitrary; here is illustrated a case in which one ICI carrying similar undesirable information is zeroed for every projection direction. Finally, projection images are ICA-reconstructed from the selected ICIs (here, two for every projection direction). 3D image is reconstructed using the ICA reconstructed projection images; this can be done using all or only select sets of the ICA reconstructed projection images, as desired.

2.3 2D Simulations

To simulate CT image processing in a 2D case (Fig. 2), a human head model slice image was obtained from the MATLAB function `phantom` using a simplified head model. To simulate imagings with different CT settings, object intensities within the slice images were modified ad hoc for each simulated imaging (Fig. 2 Column B). The function `radon` was used to generate 1D projections at 1600 directions equispaced around the slice. Exemplary projections are shown in Fig. 2 Column A. Three tests were conducted: with noiseless images (Fig. 2 Column B), images with slight but different noise added to each mage (noisy originals not shown), and images with the same strong Gaussian uniformly distributed noise added to every image (Fig. 2 Column E); this last case is unnatural but illustrates the workings of ICA.

ICA was calculated over the sets of three projections, i.e., $\mathbf{Y}_i$ (1) had three rows (e.g., the projections in Fig. 2 Column A, one projection per row). All projections $\mathbf{Y}_i$' were reconstructed using (2) with only one of IC at a time, i.e., $\mathbf{X}_i$' (2) had only one non-zero row for each ICA reconstruction. This was done separately for each of the 1600 projection directions (c.f., Fig. 1). Finally, a slice image was reconstructed from each set of 1600 reconstructed projections. This was done separately with all three sets of ICA reconstructed projections, resulting in three slice images (c.f., Fig. 2 columns C, D, and F).

2.4 µCT Imaging

We used Xradia MicroXCT-400 (Carl Zeiss Microscopy GmbH, Jena, Germany) with a 4X objective resulting in the pixel size of 44.64 µm. For each 3D image, we acquired 1600 projection images at equispaced angles around the object. The images were cropped to 271x401 to ease ICA processing for demonstration purposes. Four different 3D imageries were acquired: at 80 kV and 10 W, 80 kV and 6W, 40kV and 10 W, and 40 kV and 6W. The change in power affected the resulting noise variance, and the change in voltage the photon energy resulting in different absorption characteristics.

2.5 The Phantom

The phantom (c.f., Fig. 3) consisted of a 1 ml syringe filled with water and four polylactic acid (PLA) and two acrylonitrile butadiene styrene (ABS) filaments. Both filaments are common 3D printer materials. Some air bubbles persisted in the tube.

2.6 ICA of the µCT Projection Imagery

The real µCT 3D images were processed analogously to the 2D simulations. Each $\mathbf{Y}_i$ consisted of four projection images (c.f., Fig. 3 Column A), $i = 1, \ldots, 1600$. Pixel values of a 2D projection image entered in the rows of $\mathbf{Y}_i$ from left to right and from top to bottom. ICA was calculated for each $\mathbf{Y}_i$, and $\mathbf{Y}_i$' was reconstructed with all but one ICIs zeroed in each $\mathbf{X}_i$'. 3D reconstruction was performed separately for all three sets of the 1600 ICA reconstructed projection images. Exemplary 2D slices perpendicular to the imaging direction were extracted for illustration purposes (c.f., Fig. 3 Columns C and D).

3 Results

3.1 Results of ICA Processing of the Simulated Slice Image

The simulation results are shown in Fig. 2. The noiseless original simulated head slices are shown in Fig. 2 Column B, and their 1D projections (the rows of $\mathbf{Y}_i$ (1)) in Column A. The images reconstructed from ICA processed projections $\mathbf{Y}_i$**'**, with slight noise added to the original images, are shown in Fig. 2 Column C. The corresponding results for the noiseless originals are shown in Fig. 2 Column D. The extremely noisy original simulated slices are shown in Fig. 2 Column E, and the corresponding ICA processed reconstruction results in Fig. 2 Column F.

From Fig. 2 Columns C, D, and F, it is clear that ICA was able to enhance the round region that could not be seen in the original images. In the noise free case (Fig. 2 Column D), this region was quite well separated in an ICs of its own, whereas in the slightly noisy case (Fig. 2 Column C), the corresponding ICs contained contributions also from object edge regions. In the very noisy case (Fig. 2 Columns E and F), the noise quite completely overshadowed the two oval objects, which are probably still embedded in

the last reconstructed slice image in Fig. 2 Column F. Still, the round object was nicely separated.

According to our experimentation, the process is noise sensitive. Only low noise levels could be tolerated to recover the round object (Fig. 2 Column C, middle image) when the noise differed between the original images, as it would in reality. In case of the same noise affecting every original image (Fig. 2 Column E), the noise was well captured in one set of ICs (Fig. 2 Column F, bottom image) and could thus be removed, whereas another set of ICs clearly carried the round object (Fig. 2 Column F, uppermost image). The oval objects, however, were not observable; this was probably due to a higher number of true ICs than available measurements.

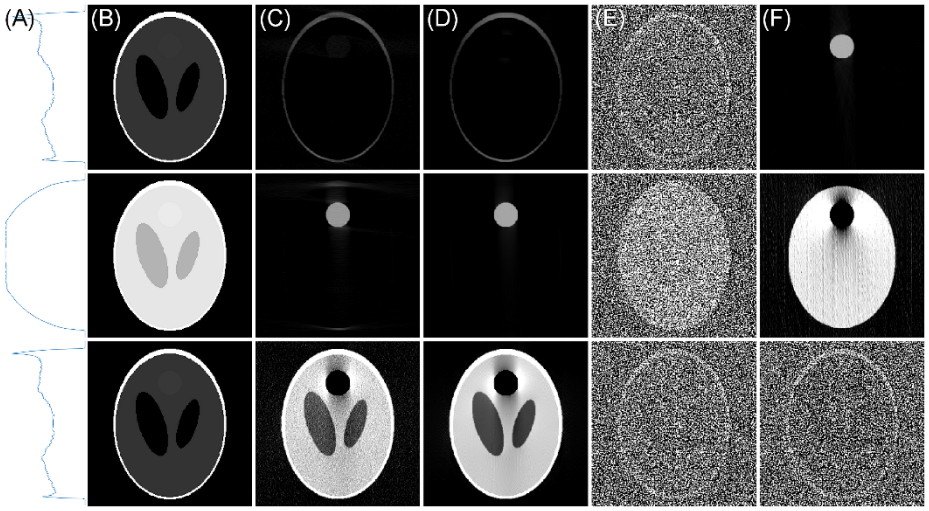

Fig. 2. The simulations and ICA processing results. Column A: Exemplary 1D projections of the original phantom images in Column B. Column C: Slice images reconstructed from ICA processed slightly noisy projections of the slice images in Column B. Column D: Slice images reconstructed from ICA processed noiseless projections of the slice images in Column B. Column E: Highly noisy original phantom images (the same noise in each). Column F: Slice images reconstructed from ICA processed projections of the slice images in Column E.

3.2 Results of ICA Processing of the 3D Phantom Projection Imagery

µCT 3D image processing results are shown in Fig. 3. An exemplary projection image for each of the four imagings with different device settings is shown in Fig. 3 Column A. The corresponding ICIs are shown in Fig. 3 Column B, where noise along with some object features were nicely extracted into the two bottom ICIs, whereas the actual object image information was captured mostly in the two uppermost ICIs.

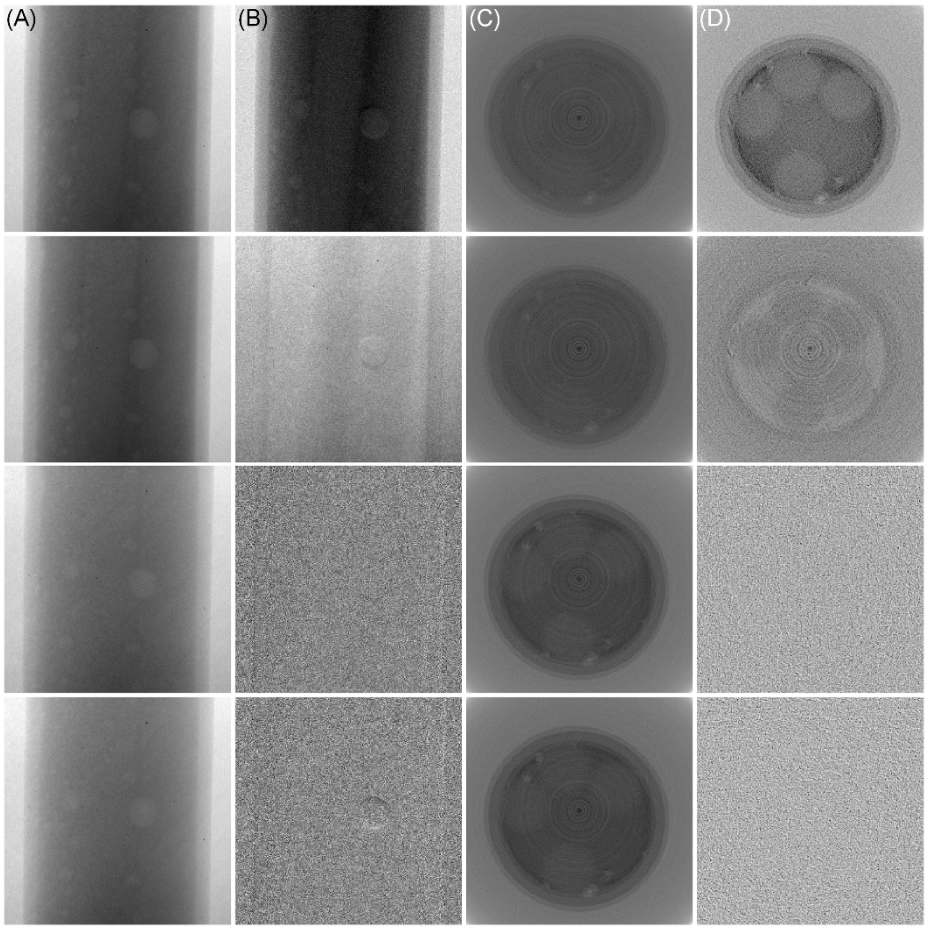

Fig. 3. µCT images and ICA processing results. Column A: Exemplary projection images taken using the four sets of µCT imaging parameters. Column B: Reconstructed ICIs. Column C: Slices of the 3D reconstructions from the raw imaging data. Column D: Slices of the 3D reconstructions from the reconstructed ICIs. The images in Columns C and D have been brightened equally for readability.

An exemplary horizontal slice of the 3D reconstructions of the phantom for the different device settings is shown in Fig. 3 Column C with the corresponding slice from 3D reconstructions made from the ICA reconstructed ICIs in Column D. Although the slice images of the original 3D reconstructions (Fig. 3 Column C) are of quite low contrast and the filaments are not always observable, the contents of the phantom are visually detectable in the slice images produced with the proposed method (Fig. 3 Column D).

After our ICA-based processing (Fig. 3 Column D), two different phantom materials can be distinguished: in the uppermost image, four round objects are clearly observable, whereas in the second image at least five round objects are observable (the object in the

middle is obscured by the imaging artefact). From slice images reconstructed without ICA processing (Fig. 3 Column C), the existence of two different materials cannot be observed.

The slice of the two last 3D constructions in Fig. 3 Column D seem to carry mostly noise; these noise components were eliminated from the other reconstructed 3D images.

4 Conclusions

We conclude that ICA processing of multispectral/multienergy X-ray tomography projection images is a potential tool for noise alleviation, object separation, and to distinguish materials in 3D CT reconstructions. However, to enable separation of more image objects and to improve noise alleviation, more image sets with different CT parameters should be available than used here. For object separation, low-noise CT imagery would be preferable.

The proposed method is completely general, and we expect it to be beneficial in several applications, including in enhancing complex biomedical and industrial imagery.

Conflict of Interest Declaration

No conflict of interest.

Acknowledgments

The work of J. M. A. Tanskanen has been supported by Jane and Aatos Erkko Foundation, Finland, under the project Biological Neuronal Communications and Computing with ICT. The work of M. Hannula has been supported by the Human Spare Parts Project funded by Finnish Funding Agency for Technology and Innovation (TEKES).

References

1. Cierniak, R.: X-ray Computed Tomography in Biomedical Engineering. Springer, London (2011). https://doi.org/10.1007/978-0-85729-027-4
2. Hyvärinen, A., Karhunen, J., Oja, E.: Independent Component Analysis. John Wiley & Sons, NY (2001). https://doi.org/10.1002/0471221317
3. Hyvärinen, A.: Fast and robust fixed-point algorithms for independent component analysis. IEEE T. Neural Networ., 10(3), 626–634 (1999). https://doi.org/10.1109/72.761722
4. Hyvärinen, A., Oja, E.: Independent component analysis: algorithms and applications. Neural Networks, 13(4–5), 411–430 (2000). https://doi.org/10.1016/S0893-6080(00)00026-5
5. Tang, S., Wang, Y., Chen, Y.-W.: Application of ICA to X-ray coronary digital subtraction angiography. Neurocomputing 79, 168–172 (2012). https://doi.org 10.1016/j.neucom.2011.10.012

6. Chen, Y. W., Han, X., Oikawa, S., Fujita, A.: Independent component analysis for removing X-ray scatter in X-ray images. In Conf. Proc. 2007 IEEE Instrumentation and Measurement Tech. Conf., pp. 1–4. IEEE, Piscataway, NJ (2007). https://doi.org/10.1109/IMTC.2007.379278
7. FastICA package for Matlab, http://www.cis.hut.fi/projects/ica/fastica/, last accessed 2019/04/18.
8. Hu, X., Shimizu, A., Kobatake, H., Nawano, S.: Independent component analysis of four-phase abdominal CT images. In Barillot, C., Haynor, D. R., Hellier, P. (eds.) Medical Image Computing and Computer-Assisted Intervention, LNCS, vol. 3217, pp. 916–924. Springer, Heidelberg, Germany (2004). https://doi.org/10.1007/978-3-540-30136-3_111
9. Jolliffe, I. T.: Principal component analysis. Springer, NY (2002). https://doi.org/10.1007/b98835
10. Tanskanen, J. M. A., Viik, J. J.: Independent component analysis in ECG signal processing. In: Millis, R. M. (ed.) Advances in Electrocardiograms, pp. 349–372. InTech, Rijeka, Croatia (2012). https://doi.org/10.5772/22719